European Journal of Medicinal Chemistry 160 (2018) 94–107

Contents lists available at ScienceDirect

European Journal of Medicinal Chemistry

journal homepage: http://www.elsevier.com/locate/ejmech

Research paper

# A road map for prioritizing warheads for cysteine targeting covalent inhibitors

Péter Ábrányi-Balogh [a], László Petri [a], Tímea Imre [b], Péter Szijj [a], Andrea Scarpino [a], Martina Hrast [c], Ana Mitrović [c], Urša Pečar Fonovič [c], Krisztina Németh [d], Hélène Barreteau [e], David I. Roper [f], Kata Horváti [g], György G. Ferenczy [a], Janko Kos [c], Janez Ilaš [c], Stanislav Gobec [c, **], György M. Keserű [a, *]

[a] Medicinal Chemistry Research Group, Research Centre for Natural Sciences, Hungarian Academy of Sciences, Magyar tudósok krt 2, H-1117, Budapest, Hungary
[b] MS Metabolomics Research Group, Research Centre for Natural Sciences, Hungarian Academy of Sciences, Magyar tudósok krt 2, H-1117, Budapest, Hungary
[c] Faculty of Pharmacy, University of Ljubljana, Aškerčeva cesta 7, SI-1000, Ljubljana, Slovenia
[d] Chemical Biology Research Group, Research Centre for Natural Sciences, Hungarian Academy of Sciences, Magyar tudósok krt 2, H-1117, Budapest, Hungary
[e] Equipe Enveloppes Bactériennes et Antibiotiques, Institut de Biologie Intégrative de la Cellule (I2BC) UMR 9198 CEA-CNRS-UPSud, Bâtiment 430, Université Paris-Sud, F-91405, ORSAY Cedex, France
[f] School of Life Sciences, University of Warwick, Gibbet Hill Road, Coventry, West Midlands, CV4 7AL, United Kingdom
[g] MTA-ELTE Research Group of Peptide Chemistry, Hungarian Academy of Sciences, Eötvös Loránd University, H-1117, Budapest, Hungary

ARTICLE INFO

*Article history:*
Received 17 July 2018
Received in revised form
7 September 2018
Accepted 3 October 2018
Available online 6 October 2018

*Keywords:*
Covalent inhibitors
Electrophilic warheads
GSH reactivity assay
Oligopeptide specificity assay
MurA
Cathepsin B
Cathepsin X

ABSTRACT

Targeted covalent inhibitors have become an integral part of a number of therapeutic protocols and are the subject of intense research. The mechanism of action of these compounds involves the formation of a covalent bond with protein nucleophiles, mostly cysteines. Given the abundance of cysteines in the proteome, the specificity of the covalent inhibitors is of utmost importance and requires careful optimization of the applied warheads. In most of the cysteine targeting covalent inhibitor programs the design strategy involves incorporating Michael acceptors into a ligand that is already known to bind non-covalently. In contrast, we suggest that the reactive warhead itself should be tailored to the reactivity of the specific cysteine being targeted, and we describe a strategy to achieve this goal. Here, we have extended and systematically explored the available organic chemistry toolbox and characterized a large number of warheads representing different chemistries. We demonstrate that in addition to the common Michael addition, there are other nucleophilic addition, addition-elimination, nucleophilic substitution and oxidation reactions suitable for specific covalent protein modification. Importantly, we reveal that warheads for these chemistries impact the reactivity and specificity of covalent fragments at both protein and proteome levels. By integrating surrogate reactivity and selectivity models and subsequent protein assays, we define a road map to help enable new or largely unexplored covalent chemistries for the optimization of cysteine targeting inhibitors.



## 1. Introduction

Targeted covalent inhibitors (TCIs) are typically high affinity compounds that selectively block the activity of the targeted proteins by forming covalent bonds with nucleophilic amino acid residues [1]. The nucleophilic partner is most often cysteine; however, other residues, such as serine, threonine, tyrosine and lysine, can also be considered [2]. The importance of cysteine-targeting is supported by the low occurrence of cysteine in the human proteome (2.3%) [3] that alleviates selectivity issues and the low conservation of non-catalytic cysteines particularly in protein

* Corresponding author.
** Corresponding author.
*E-mail addresses:* Stanislav.Gobec@ffa.uni-lj.si (S. Gobec), keseru.gyorgy@ttk.mta.hu (G.M. Keserű).

https://doi.org/10.1016/j.ejmech.2018.10.010
0223-5234/

kinases is also advantageous for selectivity and for avoiding the development of resistance [4]. The cysteine thiol is highly reactive due to its high electron density and polarizability. Therefore, it can be attacked with low reactivity ligands that is preferred to minimize side-effects [3,5]. Moreover, cysteines play a significant role in a variety of functions including nucleophilic and redox catalysis, metal binding and allosteric regulation. These functional cysteines are found on diverse proteins such as proteases, oxidoreductases and kinases and therefore cysteine-targeted electrophiles can be utilized to affect the function of a wide range of proteins [6–9]. Covalent inhibitors can possess several advantages over non-covalent, reversible compounds [10,11], including having high potency combined with high biochemical efficiency due to the complete and non-equilibrium-based inhibition of the target. The high specificity and potency of the inhibitors can translate to lower and less frequent dosing with decreased potential for off-target effects. Covalent binding also results in long residence times on the target [12], which manifests in extended durations of action. Covalent binders can enhance target occupancies and maintain target engagements that improve the therapeutic utility of compounds with limited plasma levels, which can contribute to the management of drug resistance [13]. Early phase drug discovery programs can also benefit from a targeted covalent approach providing small molecule probes and viable chemical starting points for challenging targets of low tractability. However, irreversible inhibitors are often systematically removed during screening cascades due to a number of risk factors, including reactive metabolites, drug-induced toxicity and immunogenicity [14]. Consequently, reactivity and specificity have major impacts on the fate of TCIs and should therefore be the subjects of in-depth optimization studies. Optimization of non-covalent interactions must remain in focus since non-specific binding increases the risk of unwanted side effects. Careful evaluation of the risk-benefit ratio in developing covalent inhibitors, however, should obviously include the optimization of their chemical reactivity. The difficulties of drug discovery research with lead compounds that have reactive metabolites [15] suggest that highly reactive electrophiles are not suitable warheads for covalent inhibitors. Therefore, TCIs are typically equipped with weakly reactive or even reversible warheads [16], which – in the case of cysteine targeted molecules – have introduced a clear bias towards Michael additions. A recent analysis of cysteine targeting covalent inhibitors suggests that almost 70% of the published compounds have Michael acceptor-type warheads, with acrylamides being the predominant functional group (Supplementary Fig. S1) [17]. This tendency has resulted in an actual design paradigm of putting more emphasis on the optimization of the initial non-covalent interactions and then adding warheads from known covalent inhibitors [18]. Following the identification of a suitable reversible inhibitor with a known binding mode, this strategy then focuses on the correct positioning of the selected reactive functionality. Given the electronic crosstalk between the non-covalent scaffold and the warhead, this approach prevents the parallel optimization of covalent and non-covalent interactions and keeps the discovery of novel inhibitors biased towards already proven covalent chemistries, particularly the over-represented Michael addition. A decidedly greater variety of electrophiles can be found, for example, in natural products, which cover a much wider range of chemistries, including both Michael-type ($Ad_{NM}$) and non-Michael ($Ad_N$)-type nucleophilic additions, addition-elimination reactions (Ad-E), nucleophilic substitutions ($S_N$) and oxidations (Ox) [19]. To the best of our knowledge, the potential to use all these chemistries in the design of TCIs has not been investigated systematically.

Here, we use a large set of different warheads representing a wide range of chemistries to explore their effect on reactivity and selectivity towards cysteine, the most frequently targeted protein nucleophile. Deciphering the impact of warhead chemistries, we investigate covalent fragments [20–22] that typically form only a few non-covalent interactions with a target [23]. We therefore constructed a covalent fragment library with diverse warhead chemistries and investigated its reactivity against glutathione (GSH), an oligopeptide model with multiple nucleophilic residues and intact proteins. Furthermore, our approach suggests changes in the design strategy of TCIs, as screening covalent fragments would allow selecting and optimizing an appropriate warhead that could be developed further using the established methodologies of fragment-based drug discovery [24]. Our results revealed that $Ad_N$, Ad-E, $S_N$, and oxidation reactions cover the same range of reactivity in a biological environment as Michael additions and that they perform with different levels of reactivity and selectivity in surrogate peptide models, in full proteins and in living cells. Furthermore, we extended the concept of reversible covalent inhibition to new groups of electrophilic warheads. The protocols and extensive experimental data discussed here provide a road map for the selection of cysteine targeting warheads specifically tailored for the targeted protein.

## 2. Results and discussion

### 2.1. Reactivity profiling of electrophilic warheads

Based on the available reactions of sulphur nucleophiles, particularly thiols and thiolates, we constructed a fragment library for covalent modification of cysteine residues in proteins. In addition to $Ad_{NM}$, we considered other $Ad_N$, Ad-E, $S_N$ reactions and oxidations (Fig. 1).

Our design principles consist of diverse types of warheads that are each represented by, on average, four examples with small but structurally diverse fragment scaffolds. In total, we selected 137 chemical probes with 36 different warheads with an average heavy atom count of $13 \pm 5$ and a molecular weight of $180 \pm 66$ Da (see Supplementary Fig. S2 for chemical structures).

To evaluate the cysteine reactivity of the fragments, a kinetic assay was performed using the tripeptide glutathione (GSH) as the surrogate cysteine thiol source (see Fig. 2 and Supplementary Table S1) [20] that is an indicator for promiscuous covalent binding [25].

Reactions were conducted with a large excess of GSH to ensure pseudo first order kinetics, and so linearity in the consumption of the fragments. Following ref. [20] we used the stable and non-interfering indoprofen as an internal standard in MS analysis. Additional control experiments were performed without GSH to characterize the aqueous stability of the probes. The GSH assay resulted in $\ln(AUC/AUC_0)$ versus t curves (curve I on Fig. 2) determined by linear regression, where the slope was equal to $-(k_{GSH} + k_{degradation})$. The blank assay provided $k_{degradation}$ in a similar way (curve II on Fig. 2), and the data, together with the time course of fragment reactivity (curve III on Fig. 2), allowed the GSH reactivity of a fragment to be calculated in terms of half-life $t_{1/2} = \ln 2/k_{GSH}$.

The resulting $t_{1/2}$ values were used to quantitatively characterize the reactivity of the library members. Across all fragments, 64 were found to be reactive, representing 22 warhead types from the five chemistry subsets. Of those 22 warhead types, 10 reacted as Michael acceptors (**I-X**, Fig. 1), 5 reacted in non-Michael additions (**XII-XVI**), 1 warhead reacted in an Ad-E (**XIXa**), 4 warheads participated in $S_N$ reactions (**XXV-XXVIII**), and 2 warheads were reacting in oxidation reactions (**XXXII** and **XXXIII**). In the case of Michael acceptors, sterically hindered acrylamides (**IIIb**) and a halogenated α,β-unsaturated oxo compound (**XI**) did not react with GSH under the applied conditions. Of the $Ad_N$ warheads, the oximes

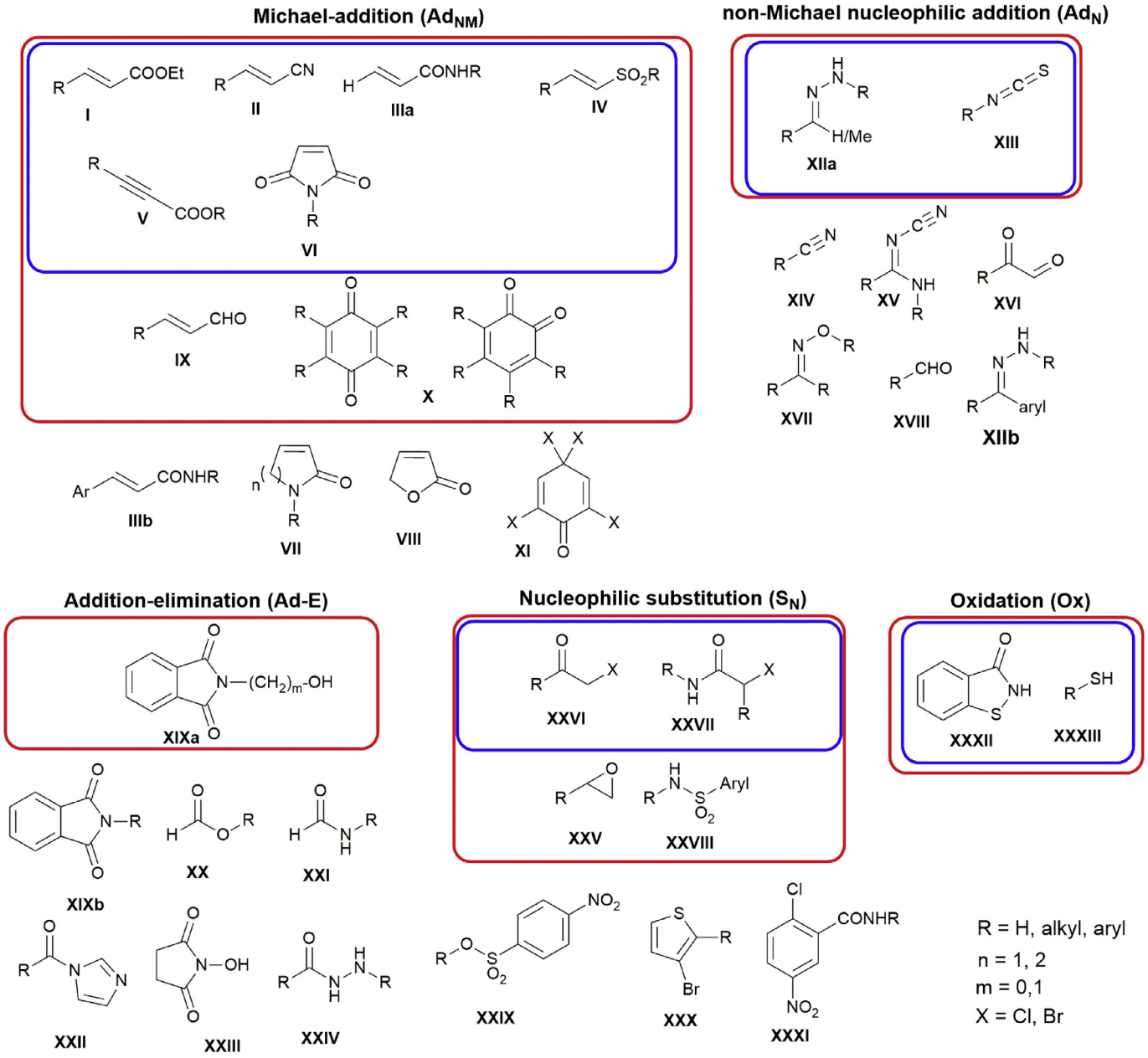


**Fig. 1.** General structure of the electrophilic library sorted by warhead chemistries. Red and blue boxes indicate GSH-reactive and cysteine-selective warheads, respectively. (For interpretation of the references to colour in this figure legend, the reader is referred to the Web version of this article.)

(**XVII**), aldehydes (**XVIII**) and sterically hindered hydrazones (**XIIb**) showed no reactivity, and from the Ad-E and $S_N$ subsets, the phthalimides (**XIXb**), formates (**XX**), formamides (**XXI**), imidazoamides (**XXII**), *N*-hydroxysuccinimide (**XXIII**), hydrazides (**XXIV**), sulfonesters (**XXIX**), halothiophenes (**XXX**), and electron poor chlorobenzenes (**XXXI**) showed no reactivity. From the set of reactive fragments, 45 reacted in an appropriate time scale with GSH reactivities of $t_{1/2} < 50$ h [26]; representing 17 warheads.

The GSH half-lives of some Michael acceptors, including cyclic acrylamides (**VII**), acrylesters (**VIII**), the non-Michael type nitriles (**XIV**), imino nitriles (**XV**) and the Ad$_N$ type glyoxyl warheads (**XVI**), were outside the criteria. Given the incubation time of <60 min in most of the fragment screens [27], we chose a buffer stability criterion of $t_{1/2}$ of degradation greater than 1 h that kicked off one fragment and ultimately resulted in a pool of 44 fragments representing 17 different warheads. We compared the reactivity ranges observed and concluded that not only do Michael-additions satisfy the appropriate reactivity criteria [26], but all of the other four chemistries provided warheads with similar reactivity profiles (see Supplementary Fig. S3 for GSH $t_{1/2}$ values by chemistries). Moreover, we found significant overlap of the reactivity distributions obtained for the different chemistries (Fig. 3) indicating that other chemistries in addition to Michael additions are suitable for the optimization of TCI reactivities against cysteines.

Detailed analysis of the results revealed that the warheads reacting most readily with GSH (**VI**, **X**, **XIII**, **XXV** and **XXXII**) were part of the Ad$_{NM}$, Ad$_N$, $S_N$, and Ox subsets, and fragments with the lowest suitable reactivity ($24\ h < t_{1/2} < 50\ h$) were compounds such as the acrylic esters (**I**) and acrylonitriles (**II**), hydrazones (**XIIa**), *N*-hydroxy(methyl)phthalimides (**XIXa**) and haloacetamides (**XXVII**),

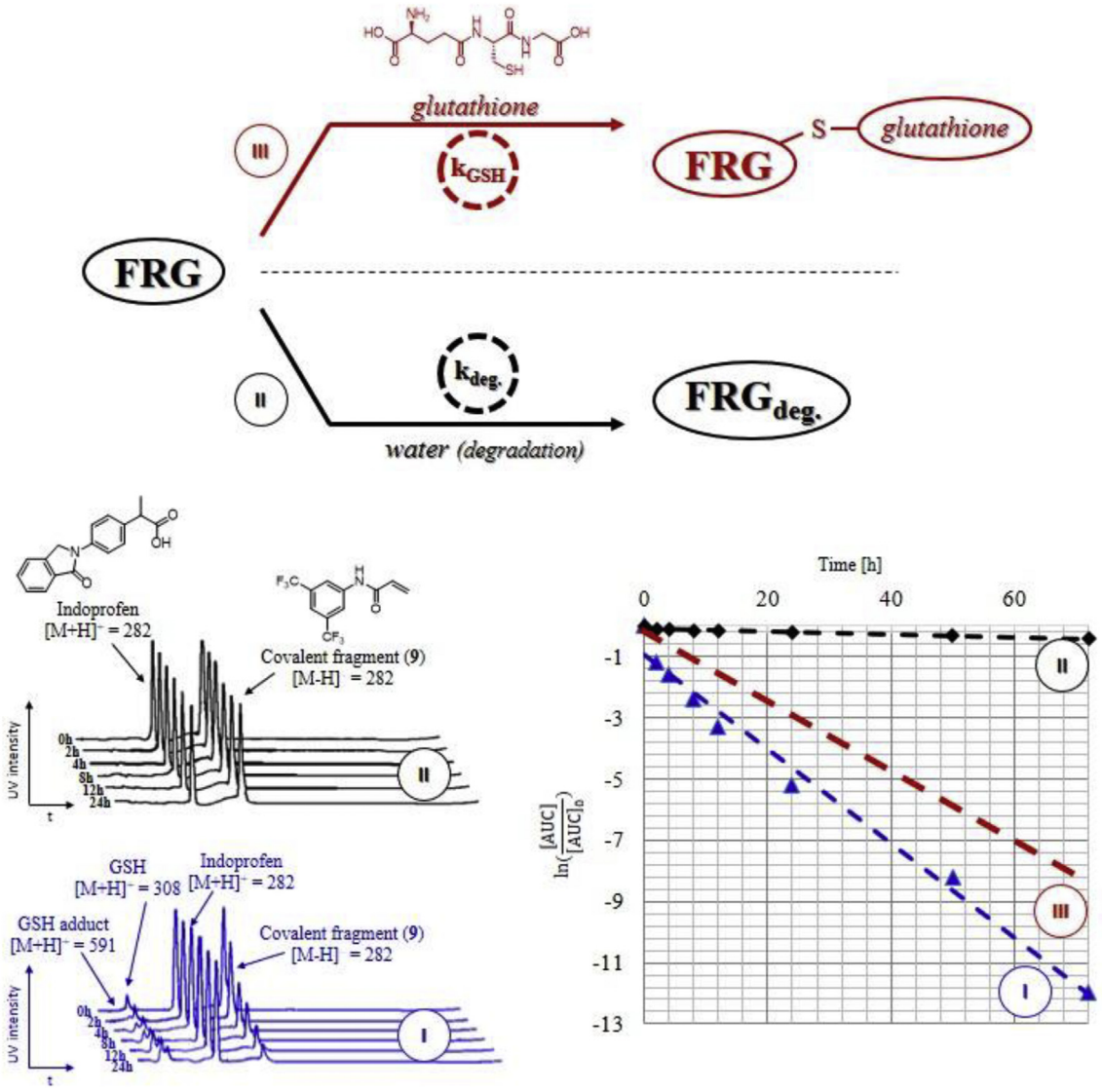


**Fig. 2.** Kinetic profiling of a representative covalent fragment (**9**) against GSH by LC-MS. LC-MS spectra were recorded at 0, 2, 4, 8, 12, 24, 48 and 72 h time points. Curves I, II and III show the measured fragment consumption, the measured aqueous stability of the fragment, and the calculated fragment reactivity, respectively.

from the $Ad_{NM}$, $Ad_N$, Ad-E, and $S_N$ warhead groups, respectively.

After exploring their GSH reactivity and aqueous stability, we then investigated whether the reactive fragments are selective towards cysteine or also reactive to other nucleophilic residues. We envisioned accomplishing this using an assay with an oligopeptide (KGDYHFPIC nonapeptide, NP) designed for this particular assay that contains lysine, tyrosine and histidine in addition to the targeted cysteine. Having confirmed the covalent binding of the fragments to the NP with LC-MS/MS measurements, it was then possible to assess their selectivity. This study provided evidence that 28 of the 44 fragments, representing 12 of the 17 warheads, were cysteine selective, based on the criterion, that the electrophilic fragment should show at least 3-fold reactivity towards cysteine in the tested 1 mM concentration as compared to any other residue of the nonapeptide.

Warheads **XVI** and **XIXa**, which react by $Ad_N$ and Ad-E, respectively, were exclusively lysine selective. Michael acceptor quinones (**X**) reacted rapidly and showed no selectivity at all. Epoxides (**XXV**) labelled cysteine, but also significant lysine-reactivity was observed. Some of the maleimides (**VI**) and isothiocyanates (**XIII**) also appeared to show minor reactivity with lysine, while acrylic aldehydes (**IX**) gave exclusively lysine adducts, presumably reacting at the aldehyde carbonyl instead of the C=C double bond. Some α-halogenated oxo-compounds (**XXVI**) and a vinyl sulfone (**IV**) reacted slightly with the tyrosine residue in addition to cysteine. Nitriles (**XIV**) and iminonitriles (**XV**) showed modest GSH reactivity and no reaction in the oligopeptide assay. The conversion of reaction with the NP corresponded to GSH half-lives (Spearman Rho = 0.73) within the given chemistry and warhead subsets, which confirms the predictive power of these early roadmap assays. The most reactive warheads were the haloacetophenones (**XXVI**), epoxides (**XXV**), haloacetamides (**XXVII**) and maleimides (**VI**), representing the $S_N$ and $Ad_{NM}$ types of reactions. In summary, starting from the large set of chemical probes representing a diverse set of potential cysteine targeted warheads, we identified 44 reactive and stable fragments (constituting 17 warheads), 28 (constituting 12 warheads) of which were found to be cysteine selective (Fig. 4, Supplementary Tables S1 and S2). Furthermore, we have elongated NP with a terminal Thr (TKGDYHFPIC), that is a relevant nucleophilic residue

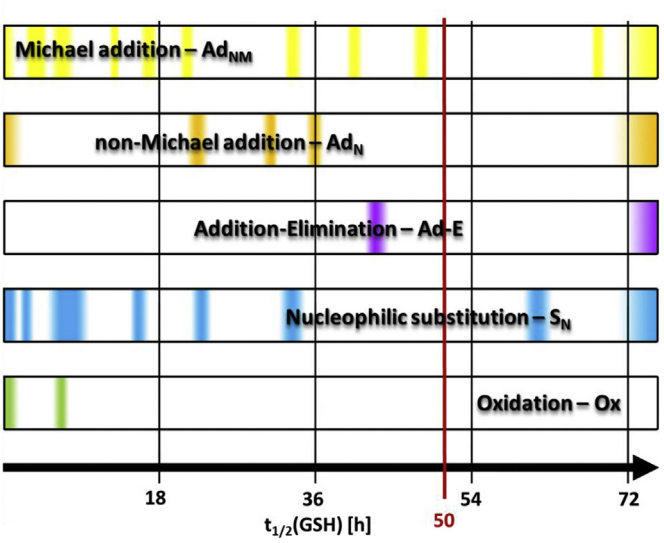


**Fig. 3.** GSH reactivity distribution of different chemistries. Warheads **I-X** and **XIIa-XVI** represent the $Ad_{NM}$ and $Ad_N$ type nucleophilic additions, respectively. Reactivity of warheads **XIXa**, **XXV-XXVIII** and **XXXI-XXXII** is depicted for Ad-E, $S_N$ and Ox reactions, respectively. The coloured lines represent the GSH half-lives of fragments in the corresponding warhead chemistries showing that a suitable reactivity range can be covered by multiple chemistries.

mainly in the proteasome field [28] and developed a decapeptide assay for testing the cysteine selective fragents. This study revealed that most of the cysteine selective fragments showed no reactivity against Thr, only fragment **46** (**XIII**) that is strongly activated by a nitro group, showed less than 3-fold reactivity towards cysteine (Supplementary Table S1).

We showed that in addition to Michael acceptors, warheads of $Ad_N$, $S_N$ and Ox reactions can be considered in the design of TCIs. In addition, our results suggest that the combination of aqueous stability, GSH reactivity and oligopeptide selectivity assays is a feasible way to discover and optimize warheads for covalent inhibitors.

### 2.2. Protein level reactivity of covalent fragments

Cysteine-reactive and chemically stable covalent fragments profiled by the GSH reactivity and the oligopeptide selectivity tests were then evaluated in an enzyme inhibition assay against MurA (UDP-N-acetylglucosamine enolpyruvyl transferase), an enzyme that catalyses the first committed step of bacterial peptidoglycan biosynthesis. MurA is generally considered a promising antibacterial target since it is expressed by both Gram-positive and Gram-negative bacteria, it has no mammalian orthologue, and it is clinically validated [29]. Despite intense research, relatively few compounds have been described as potent MurA inhibitors [30,31]. Fosfomycin is the only clinically available MurA inhibitor that binds covalently to the Cys115 residue in the active site. The inhibitory activity of the 27 GSH reactive covalent fragments showing appropriate aqueous stability was tested at a concentration of 100 μM against MurA from *Escherichia coli* ($MurA_{EC}$) in the presence and absence of 0.1 mM dithiothreitol (DTT). Since DTT reacts with electrophilic compounds, their warheads are no longer available to react with Cys115 of $MurA_{EC}$. Without the covalent interaction, the fragments do not inhibit the enzyme, making it possible to decouple covalent binding from non-covalent interactions. Comparative analysis of the results showed that most of the fragments bind covalently to the target (Fig. 5).

As expected, it was found that fragments with different warheads performed differently. Focusing on the actives (identified as those producing a residual enzyme activity (RA) less than 80% at 100 μM of compound), we identified warheads in all four tested chemistry classes ($Ad_{NM}$, $Ad_N$, $S_N$, and Ox) (Fig. 5).

The median activity of actives was highest for oxidations, followed by nucleophilic substitutions and non-Michael type nucleophilic conjugate additions. At the warhead level (Fig. 5 and see Table 2 for numeric data), haloacetophenones (**XXVI**) and isothiocyanates (**XIII**) were more active than haloacetamides (**XXVII**), and hydrazone (**XIIa**). Covalent fragments equipped with Michael acceptor warheads had varying inhibitory potencies. Maleimides (**VI**) were the most reactive Michael acceptors, showing activities similar to the best $S_N$ type warheads, followed by vinylsulfone (**IV**, **15**) and butynoate (**V**, **19**). Acrylesters (**I**), acrylonitriles (**II**) and

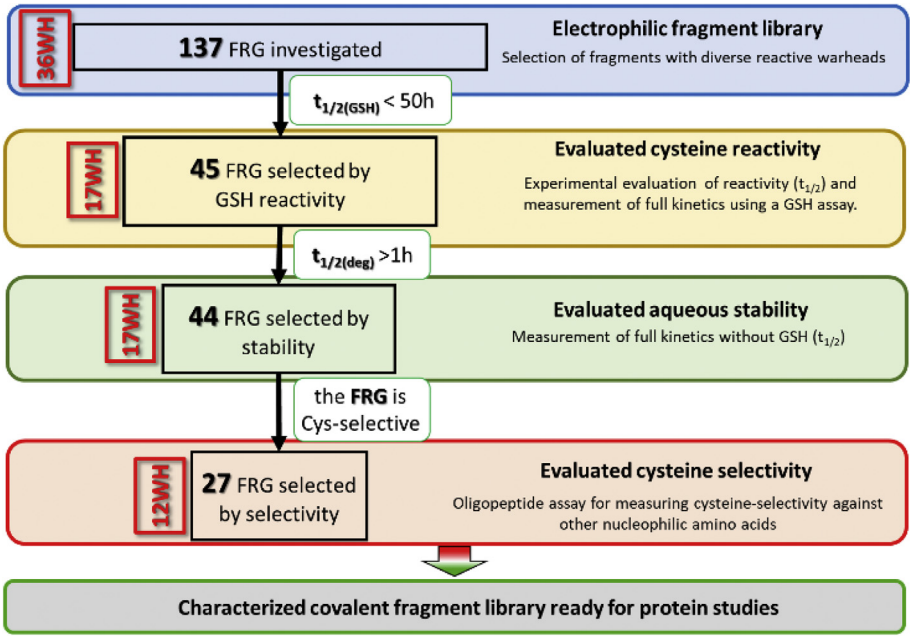


**Fig. 4.** Generation of the covalent screening library.

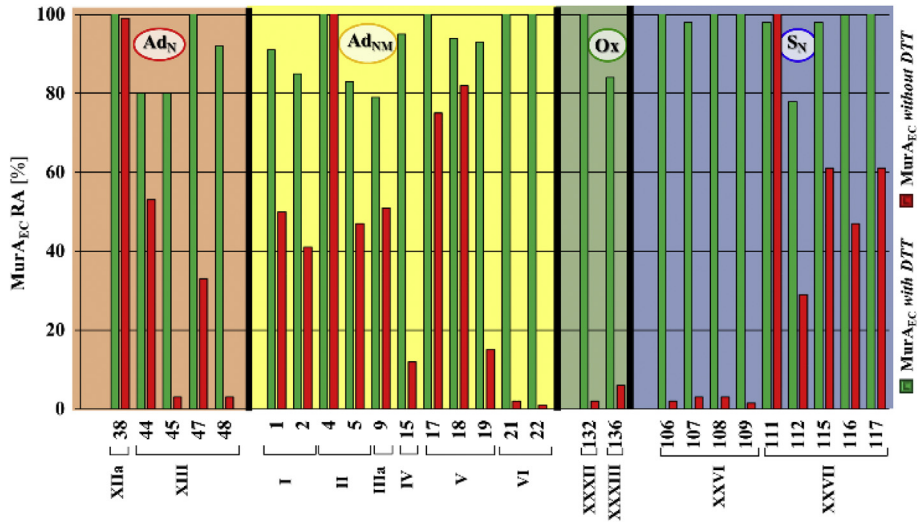


**Fig. 5.** Characterization of the protein reactivity with covalent fragments having different warhead chemistries. Inhibition of $MurA_{EC}$ by covalent fragments, measured in the presence (green) and absence (red) of DTT, presented as residual activity of the enzyme in the presence of 100 μM concentration of fragment. Chemistries are indicated with background colours according to $Ad_N$ (orange), $Ad_{NM}$ (yellow), Ox (dark green) and $S_N$ (blue). Median potency of actives by warhead chemistries is also indicated. (For interpretation of the references to colour in this figure legend, the reader is referred to the Web version of this article.)

**Table 1**
Inhibitory activity and inhibition mechanism of covalent fragments against MurA[a].2

| Entry | Chemistry | Warhead | $MurA_{EC}$ $IC_{50}$ (μM) | $MurA_{SA}$ $IC_{50}$ (μM) or RA% at 100 μM | Mechanism |
|---|---|---|---|---|---|
| **44** | $Ad_N$ | **XIII** | 90 | 75% | NA |
| **45** | $Ad_N$ | **XIII** | 3.7 | 41% | I |
| **47** | $Ad_N$ | **XIII** | 45 | 91% | NA |
| **48** | $Ad_N$ | **XIII** | 28 | 53 | NA |
| **1** | $Ad_{NM}$ | **I** | 172 | 82% | R |
| **2** | $Ad_{NM}$ | **I** | 227 | 66% | NA |
| **5** | $Ad_{NM}$ | **II** | 95 | 81% | R |
| **9** | $Ad_{NM}$ | **III** | 164 | 72% | R |
| **15** | $Ad_{NM}$ | **IV** | 15 | 34 | I |
| **19** | $Ad_{NM}$ | **V** | 24 | 47 | R |
| **21** | $Ad_{NM}$ | **VI** | 0.565 | 1.04 | NA |
| **22** | $Ad_{NM}$ | **VI** | 0.554 | 0.652 | R |
| **132** | Ox | **XXXII** | 1.1 | 0.926 | I |
| **136** | Ox | **XXXIII** | 1.25 | 7.83 | NA |
| **107** | $S_N$ | **XXVI** | 0.384 | 1.82 | I |
| **108** | $S_N$ | **XXVI** | 2.25 | 3.02 | I |
| **109** | $S_N$ | **XXVI** | 5.3 | 4.12 | NA |
| **112** | $S_N$ | **XXVII** | 76 | 102 | I |
| **116** | $S_N$ | **XXVII** | 141 | 171 | I |

[a] I: irreversible and time dependent; R: reversible and time dependent; NA – not available

acrylamides (**IIIa**) showed much lower activity. The covalent fragments with the best performances were then subjected to $IC_{50}$ measurements and mechanistic studies with $MurA_{EC}$ and structurally related *Staphylococcus aureus* MurA ($MurA_{SA}$) (Table 1).

The covalent binding of different warhead types was confirmed also by MS/MS studies. Proteomics studies revealed that the maleimide **22** (**VI**, $Ad_{NM}$ type), the bromoacetophenone **107** (**XXVI**, $S_N$ type) and the benzisothiazolone **132** (**XXXII**, Ox type) form covalent bond with Cys115 located at the active site of $MurA_{EC}$ (Supplementary Fig. S4, Table S3).

**Table 2**
The effect of warhead chemistries on the functional, enzyme family, species and protein specificity. Functional specificity is illustrated by comparing the activity profiles obtained by measuring the endo- (CatB Endo) and exopeptidase (CatB Exo) functional activity of cathepsin B. The effect on enzyme family specificity is exemplified by comparing CatB Exo and the exopeptidase activity of cathepsin X (CatX) enzymes. Species specificity is shown comparing activity profiles measured for $MurA_{EC}$ and $MurA_{SA}$. Protein specificity is demonstrated by comparing $MurA_{EC}$ and cathepsin B exopeptidase activities. The activities are scaled by colours, with more active compounds (under 80% of residual activity) being shown in deeper tones. All compounds were tested in 100 μM concentration.3

| ID | Ch.[a] | WH[b] | $MurA_{EC}$ RA%[c] | $MurA_{SA}$ RA%[c] | $MurA_{EC}$ RA%[d] | CatB Endo RA%[d] | CatB Exo RA%[d] | CatX RA%[d] |
|---|---|---|---|---|---|---|---|---|
| **38** | $Ad_N$ | **XIIa** | 99 | 54 | 100 | 100 | 100 | 79 |
| **44** | $Ad_N$ | **XIII** | 53 | 75 | 91 | 100 | 98 | 67 |
| **45** | $Ad_N$ | **XIII** | 3 | 41 | 100 | 75 | 18 | 22 |
| **47** | $Ad_N$ | **XIII** | 33 | 91 | 94 | 100 | 99 | 55 |
| **48** | $Ad_N$ | **XIII** | 3 | 9 | 99 | 100 | 97 | 87 |
| **1** | $Ad_{NM}$ | **I** | 50 | 82 | 90 | 100 | 100 | 89 |
| **2** | $Ad_{NM}$ | **I** | 41 | 66 | 96 | 100 | 97 | 84 |
| **4** | $Ad_{NM}$ | **II** | 100 | 97 | 100 | 100 | 87 | 90 |
| **5** | $Ad_{NM}$ | **II** | 47 | 81 | 100 | 100 | 88 | 86 |
| **9** | $Ad_{NM}$ | **IIIa** | 51 | 72 | 100 | 92 | 90 | 92 |
| **15** | $Ad_{NM}$ | **IV** | 12 | 30 | 96 | 100 | 87 | 93 |
| **17** | $Ad_{NM}$ | **V** | 75 | 67 | 99 | 85 | 70 | 92 |
| **18** | $Ad_{NM}$ | **V** | 82 | 91 | 100 | 96 | 84 | 96 |
| **19** | $Ad_{NM}$ | **V** | 15 | 31 | 98 | 100 | 89 | 99 |
| **21** | $Ad_{NM}$ | **VI** | 2 | 0 | 99 | 100 | 87 | 96 |
| **22** | $Ad_{NM}$ | **VI** | 1 | 0.3 | 100 | 96 | 89 | 96 |
| **132** | Ox | **XXXII** | 2 | 0 | 99 | 100 | 96 | 100 |
| **136** | Ox | **XXXIII** | 6 | 23 | 94 | 100 | 67 | 100 |
| **106** | $S_N$ | **XXVI** | 2 | 7 | 94 | 83 | 27 | 95 |
| **107** | $S_N$ | **XXVI** | 3 | 4 | 100 | 90 | 55 | 74 |
| **108** | $S_N$ | **XXVI** | 3 | 7 | 93 | 63 | 34 | 86 |
| **109** | $S_N$ | **XXVI** | 1.5 | 1 | 100 | 58 | 27 | 75 |
| **111** | $S_N$ | **XXVII** | 100 | 59 | 95 | 100 | 88 | 99 |
| **112** | $S_N$ | **XXVII** | 29 | 50 | 80 | 75 | 100 | 96 |
| **115** | $S_N$ | **XXVII** | 61 | 52 | 96 | 90 | 87 | 84 |
| **116** | $S_N$ | **XXVII** | 47 | 54 | 98 | 92 | 90 | 97 |
| **117** | $S_N$ | **XXVII** | 61 | 55 | 99 | 78 | 87 | 94 |

[a]Chemistry type. [b]Warhead type. [c]Measurements without DTT. [d]Measurements with 5 mM cysteine

These studies revealed that by screening only a small set of covalent fragments, we could identify new low micromolar and even sub-micromolar MurA inhibitors that are active on both $MurA_{EC}$ and $MurA_{SA}$. The maleimide **22** and 1,2-benzisothiazol-3(2*H*)-one **132** represent novel MurA chemotypes and were among the most potent reversible or irreversible inhibitors of both MurAs, with $IC_{50}$ values similar to that of fosfomycin [32]. Interestingly, we found that a number of covalent fragments showed reversibility in binding to the $MurA_{EC}$ active site (Fig. 6, Supplementary Fig. S5 and Table S4).

Reversible covalent inhibition has been described for cyanoacrylates, cyanoacrylamides [12,16,33], electron poor heterocyclic acrylonitriles [34] and nitriles [35], but neither simple acrylates nor acrylonitriles showed reversible binding with thiols. Based on these studies, we concluded that electron withdrawing groups are needed on both sides of the double bond to make the Michael addition reversible. Here, we show that other Michael acceptor warheads (**I** (**1**), **II** (**5**), **IIIa** (**9**), **V** (**19**) and **VI** (**22**)) were also able to bind reversibly to MurA. In most cases, the thiol-reactive centre of the fragment is surrounded by electron withdrawing carbonyl (**1**, **9**, **19**, **22**) or nitrile (**5**) groups, making them similar to the electron deficient cyanoacryl derivatives. These observations suggest that a more diverse set of warheads is indeed available for reversible covalent inhibition.

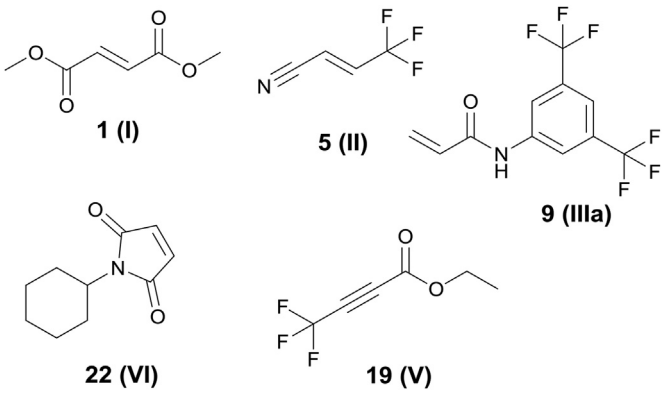


**Fig. 6.** Reversible MurA inhibitors identified by covalent fragment screening.

Next, we investigated the predictive performance of the early steps of the road map on the observed biological activity of the evaluated covalent fragments. It was found that MurA inhibitory activity follows the same trend as GSH half-life and the conversion of the oligopeptide (Fig. 7a and b).

Taken together, these data suggest that non-enzymatic models are valid predictive tools for the estimation of fragment reactivity and specificity against MurA.

### 2.3. Warhead chemistry influences target specificity

Given the demonstrated effect of warhead chemistries on cysteine reactivity, we next investigated whether the different warhead types impact functional, enzyme family, species and protein specificities. The cysteine-reactive covalent fragment set was therefore screened against cysteine peptidases such as cathepsin B and X and a non-cysteine peptidase thrombin. For the

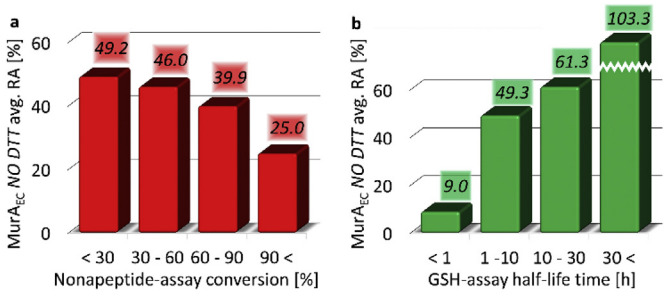


**Fig. 7.** Trend analyses of measured oligopeptide conversion (a) and GSH half-lives (b) as surrogates of $MurA_{EC}$ reactivity, respectively.

evaluation of functional specificity, we tested both endo- and exopeptidase activity of cathepsin B. The effect on the members of an enzyme family was estimated by comparing the exo activity profiles of cathepsins B and X. Species and protein specificity was analysed using the screening profiles obtained for $MurA_{EC}$ vs. $MurA_{SA}$ and $MurA_{EC}$ vs. cathepsin B exo activity vs. thrombin, respectively.

Cathepsin B is a lysosomal cysteine peptidase that has important roles in various pathological processes, including cancer, and has been validated as a promising biomarker and therapeutic target in various cancers [36–38]. The flexible occluding loop of cathepsin B exists in two characteristic conformations in which the open form is preferential for the endopeptidase activity and the closed form is preferred for the exopeptidase activity [39]. Previous studies revealed that Michael acceptors and halomethyl ketones are irreversible cathepsin inhibitors and form covalent bond with the active site cysteine [40]. The impact of different warhead chemistries on inhibitory activity and functional specificity, however, has not yet been investigated. Testing the cysteine-reactive covalent fragment library against both conformations revealed that the inhibitory activities of endo- and exopeptidase functions are dependent on the warhead chemistries (Table 2).

Our results suggest that the exopeptidase activity of cathepsin B is more sensitive to covalent fragments than the endopeptidase. Although Michael acceptors were found to be very weak inhibitors of both activities, the exopeptidase activity was more effectively inhibited by some $Ad_N$ and $S_N$ reactions and by oxidation (**XXXIII**). The warheads that were most effective in influencing either endo or exo activities utilize nucleophilic substitutions. Haloacetophenones (**XXVI**) were the most potent inhibitors of the exopeptidase activity. Interestingly, haloacetamides (**XXVII**) that also act by $S_N$ mechanisms, showed some preference for inhibiting the endopeptidase activity. Non-Michael-type additions have lower specificity coupled with limited endopeptidase inhibitory activity, except for isothiocyanate (**XIII**, **45**), which was found to be a potent and specific exopeptidase inhibitor.

Cathepsin X is yet another member of the cysteine cathepsins that is similar to cathepsin B and acts as a carboxypeptidase; however, it has narrower substrate specificity and no endopeptidase activity. This cathepsin has been associated with immune response, neuroinflammation, neurodegeneration and cancer [41,42]. Analysis of the covalent fragment hits revealed that cathepsin X is generally less sensitive to fragment electrophiles than cathepsin B (Table 2). In fact, the enzymes do not share similar activity profiles [43], that could be rationalized by the different nucleophilicity of their catalytic cysteine. Unlike with cathepsin B, the most effective cathepsin X warheads are isothiocyanates (**XIII**) that bind by $Ad_N$ reactions. Interestingly, chemically more reactive $S_N$ type warheads are virtually inactive against cathepsin X. This might suggest that cathepsin X could be more specifically targeted by an isothiocyanate type $Ad_N$ class of warheads. Again, Michael acceptors and oxidative warheads showed very limited inhibitory activity.

The effect of warhead chemistries on the same protein from different species has been investigated using MurA as an example. Analysing the sequence similarity of $MurA_{EC}$ and $MurA_{SA}$ we found only 49% of identities and 66% of positives (that is 83% and 89%, respectively within the 6 Å surrounding the reference ligand fosfomycin and the substrate UNAG), which suggests considerable differences between the proteins. Using identical assay conditions for both MurAs we compared the corresponding hit lists (Table 2). Although some Michael acceptors (**V** and **VI**), $S_N$ type and oxidative warheads showed similar inhibitory activity on MurA from both species, isothiocyanates (**XIII**) reacting with $Ad_N$ and acrylic type warheads (**I**, **II**, **IIIa**, and **IV**) were typically more active on the $MurA_{EC}$ than $MurA_{SA}$, suggesting some specificity in these warheads. This specificity can be explained by the different surroundings of the active site cysteines. In $MurA_{EC}$ Cys115 is followed by a Thr while the residue next to the active cysteine in the $MurA_{SA}$ homologue is Ala. Furthermore, there is another structural difference in the catalytic loops (Ala119 in *E. coli* vs. Ser123 in *S. aureus*). Comparison of the $MurA_{EC}$ crystal structure (1HUC) to the homology model of $MurA_{SA}$ [44] showed that steric effects are less important. Shape similarity of the active sites, however, suggests that the catalytic cysteine of $MurA_{EC}$ might have a more nucleophilic character than that of the $MurA_{SA}$. Interestingly, the other $Ad_N$ type warhead, hydrazone **38** (**XIIa**), was more active on $MurA_{SA}$, emphasizing again the impact of warhead chemistries on the species-specific inhibition of MurA.

To enable evaluation of the effect of warhead chemistries on different proteins, we compared the activities found against MurA and cathepsin B exopeptidase (Table 2). In contrast to the intracellular MurA, cathepsins are extracellular and require cysteine for their activation. To make a fair comparison, we performed the assays in similar conditions and analysed the hit lists obtained. This analysis showed that covalent fragments were more active on cathepsin B than MurA, which is in line with the lower $pK_a$ value of cathepsin B (3.4 [45] and 8.3 [46], respectively). Although $S_N$ warheads, particularly haloacetophenones (**XXVI**), were the most active on both proteins; for cathepsin B, we found differences for other chemistries. Isothiocyanate-type $Ad_N$ warheads (**XIII**) outperformed both oxidative (**XXXIII**) and Michael warheads (**I-V**) and showed the largest specificity for cathepsin B. Since both MurA and cathepsin B have a catalytic cysteine in their active sites, we also included thrombin, a serine protease, in this comparison, and it does not have such a cysteine, but a serine that can be targeted by covalent inhibitors [47]. Screening cysteine-selective covalent fragments against thrombin identified no inhibitors, consistent with the active site cysteine-specific mechanism of covalent inhibition at play here.

In summary, our analysis suggests that different warhead chemistries have a significant influence on specificity at multiple levels, including the functional activity of the same protein, the activity of different enzymes from the same family, the activity of the same enzyme from different species and the activity of different proteins. We found that these specificities are the least pronounced for $Ad_{NM}$. Interestingly, it seems that other types of chemistries, more specifically $Ad_N$ and $S_N$, provide more opportunity for specific biological responses. On the basis of these results we propose a new strategy in the design of TCIs, where the reactive warhead itself should first be optimized and tailored to the reactivity of the targeted cysteine, followed by optimization of non-covalent interactions using established methods of fragment-based drug discovery.

### 2.4. Warhead chemistry impacts proteome level reactivity and specificity

In a set of cysteine peptidases and transferases, we demonstrated that warhead chemistry influences the target specificity. A critical question is whether this observation can be validated in a larger set of proteins, more specifically at the proteome level. The recent dataset published by Cravatt et al. [48] makes this analysis feasible for two types of warhead chemistries: $Ad_{NM}$ and $S_N$. In this seminal paper, the authors investigated 52 electrophilic fragments with acrylamide (**III**, $Ad_{NM}$) and chloroacetamide (**XXVII**, $S_N$) warheads against thousands of proteins in human proteomes. By analysing the structures of covalent fragments used in this study, we found three pairs of fragments with identical scaffolds that provide a unique opportunity for unbiased comparison of different warhead chemistries (**9**–**112**, **10**–**116**, **11**–**117** shown in Fig. 8).

We therefore synthesized these fragments and tested them in the GSH reactivity and oligopeptide selectivity assays (Table 3).

Our data show that chloroacetamides (**112**, **116**, and **117**) are generally more reactive than acrylamides (**9**, **10**, and **11**) in both assays, as demonstrated by the generally lower GSH half-lives and higher oligopeptide conversions. Considering the chemical surroundings of the warheads, it seems that the electronic effects of the scaffolds impact both Michael additions and nucleophilic substitutions in a similar way. Fragments **112** and **9** were most reactive, followed by **116** and **10**, then **117** and **11**. All the fragments were cysteine-selective. We found that **11** was non-reactive in the GSH assay and that the fragment polymerized in the oligopeptide assay.

Next, we tested the fragments in the protein assays (Table 2, Supplementary Table S1). Fragments were most active against $MurA_{EC}$ and $MurA_{SA}$; they were generally much less active against the cathepsins. Acrylamides **10** and **11** were practically inactive against all of our protein targets, which is consistent with their proteome reactivity [48], represented by the % of targeted proteins (Table 3). Considering the MurA activity data, we found that $S_N$ warheads were more active than Michael acceptor **9**. MurA was most effectively inhibited by fragment **112** followed by the two other chloroacetamides (**116** and **117**), then the less active Michael acceptor (**9**). In the case of $S_N$ fragments, the trend in inhibitory activity is parallel to their GSH half-lives. However, when considering all of the probes, the inhibition potency corresponds to the proteome reactivity (Table 3). Considering the MurA activity data, we found that $S_N$ warheads were more active than Michael acceptor **9**. MurA was most effectively inhibited by fragment **112** followed by the two other chloroacetamides (**116** and **117**), then the less active Michael acceptor (**9**). In the case of $S_N$ fragments, the trend in inhibitory activity is parallel to their GSH half-lives. However, when considering all of the probes, the inhibition potency corresponds to the proteome reactivity (Table 3). Interestingly, $S_N$ type fragments **112** and **117** showed weak inhibition on the endopeptidase activity of cathepsin B but had no effect on the exopeptidase activity of cathepsin B or X. The activity profile of this set of fragments followed the general trends seen for the library. Minor alterations could be explained by their larger scaffolds, which influence the non-covalent interactions in the binding sites.

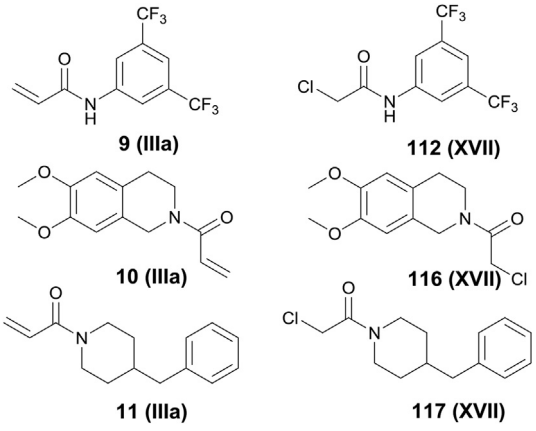


**Fig. 8.** Michael acceptors and $S_N$ type fragments with identical scaffolds investigated in MDA-MB-231 cells [48].

Proteome-level reactivity of the fragments was investigated with a subset of the MDA-MB-231 cell proteome dataset. The reactivity and specificity of covalent fragments depended on the nucleophilicity of the targeted cysteine. We therefore identified those proteins of the MDA-MB-231 dataset that were characterized in a previous study aimed at profiling the quantitative reactivity of functional cysteines in the same cell [7]. Taken the two datasets, we have compiled a cysteine reactivity annotated proteome subset for all the fragment pairs that includes 108 proteins with 124 available cysteine residues (Supplementary Tables S5 and S6). Proteome-level reactivities of the fragments were calculated from IsoTOP-ABPP ratios (Isotopic Tandem Orthogonal Proteolysis-Activity-Based Protein Profiling, R) [7]. Based on the reactivity scale used in proteome studies, we considered proteins with $R > 2$ as hits showing larger than 50% inhibition when treated with the fragments. Proteome-level reactivity followed the same trend observed for cysteine proteases, with chloroacetamides generally being more active than acrylamides. Focusing on the warhead chemistries, the proteome level data are in line with the findings in our roadmap. Among Michael acceptors, **9** was the most reactive, followed by **10** and **11**, while in the case of $S_N$ type warheads, **112** outperformed **116** and **117**. Next, we checked the influence of cysteine reactivity on the performance of covalent fragments. Cysteine reactivity was estimated using the IsoTOP-ABPP ratios (R), which are lower for more reactive cysteines [7].

Analysing the reactivity of fragments equipped with $Ad_{NM}$ and $S_N$ type warheads as a function of the reactivity of the targeted cysteines, we found that the chemistries showed remarkably distinct reactivity profiles (Supplementary Table S5). In the case of $S_N$ type fragments, the most reactive fragment (**112**) hit the most cysteines. However, the less reactive **117** outperformed **116**, which might be a consequence of steric rather than electronic effects. Michael acceptor fragments in general were found to be much less active; the most reactive fragment (**9**) targeted only four of the 50 most reactive cysteines available in the 108 proteins. More importantly, these data demonstrate that the warhead chemistry influences the reactivity and specificity of covalent fragments at the proteome level. The present analysis therefore shows that the covalent modification of cysteine residues might be specific and is dependent on the warhead chemistry, the cysteine reactivity, and relevant steric components of the molecular recognition process.

Cysteine R values were correlated to fragment reactivity data obtained for the same set of 108 proteins (Fig. 9).

In the case of $S_N$ reactions, we found that the reactivity of fragments increases with increasing nucleophilicity of the targeted cysteines. Interestingly, $Ad_{NM}$ reactions showed a different trend; in this case fragment reactivity does not increase with increasing cysteine reactivity. We also demonstrated these different trends in the reactivity of fragment pairs across the whole cysteine-reactive annotated proteome dataset (208, 179 and 158 proteins for **112** vs **9**, **116** vs **10** and **117** vs **11,** respectively, see Supplementary Table S6 and Fig. S6).

One of the most important practical consequences of this finding might be that cysteines with different nucleophilicities could be more specifically targeted by either $S_N$ or $Ad_{NM}$ warheads.

**Table 3**
The effect of warhead chemistries on reactivity and specificity at the proteome level: Reactivity differences of $Ad_{NM}$ (yellow) and $S_N$ (blue) type fragments found in the GSH reactivity and oligopeptide conversion assays, and at the proteome level.[a].4

| Fragment | GSH reactivity $t_{1/2}$ (h) | Oligopeptide conversion (α) | % of proteins targeted in MDA-MB-231 cells[48] |
|---|---|---|---|
| **9** | 4.2 | 59% | 23 |
| **10** | 86.8 | 34% | 2 |
| **11** | N.R. | deg. | 1 |
| **112** | 5.8 | 72% | 63 |
| **116** | 8 | 90% | 49 |
| **117** | 16.1 | 91% | 31 |

[a]N.R.: no reaction; deg.: degradation

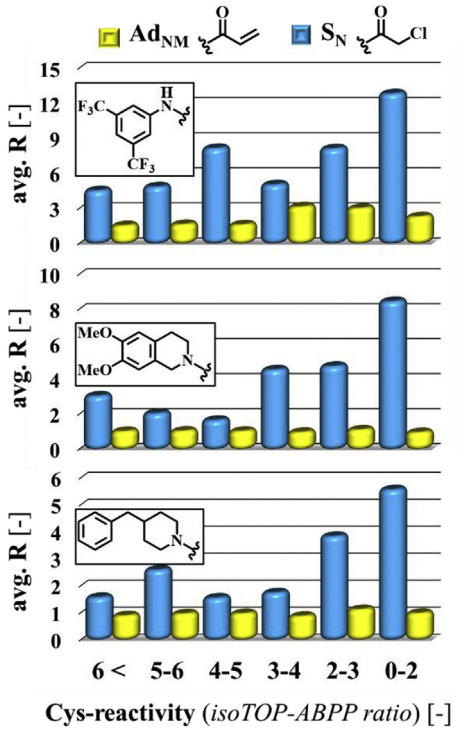


**Fig. 9.** Relationship between the proteome level reactivity and the cysteine reactivity in the 108 target proteins.

Furthermore, we can speculate that the reactivity of such warheads could be more effectively tailored for a specific cysteine of a given target. There may be multiple factors behind this opportunity. First, there are characteristic differences in the reaction mechanisms of $Ad_{NM}$ and $S_N$ warheads. Michael addition is a reversible reaction having a stepwise mechanism [49], while nucleophilic substitutions are practically irreversible and in most cases go through a highly polarized transition state [50]. Second, the protein environment influences the reaction between the warhead and the targeted cysteine. The polar environment generally favours both reactions since the high dielectric constant supports charge localization at the reaction centres [51]. Given the more polarized transition state of the $S_N$ reactions, the polar surroundings reduce the energy barrier of the reaction more effectively for $S_N$ reactions than for $Ad_{NM}$ reactions. Last, we can consider the effect of water molecules within the binding site. Hydrophobic pockets are less suited to $Ad_{NM}$ since the absence of both water- and mechanism-induced polarizing effects makes the targeted cysteine more resistant to covalent modification. In contrast, the attacking electrophile of the $S_N$ reaction can polarize the cysteine more readily, thus facilitating the formation of the covalent bond.

Post hoc analysis of proteome-level reactivity data revealed that the warhead chemistry impacts both the reactivity and specificity of covalent fragments. Although proteome data are only available for two types of chemistries, the present analysis suggests that considering the wider range of chemistries can contribute to avoiding nonspecific covalent binding and to maximizing the value of fragment based phenotypic screens [52] and covalent drug discovery programmes [10].

## 3. Conclusions

Up to now covalent drug design strategies have been more focused on optimization of non-covalent interactions and introducing a warhead from the most popular class of Michael acceptors. This strategy has led to several FDA-approved drugs, such as afatinib, tofacitinib and ibrutinib, for oncology treatments [1]. Much less attention has been paid to tailoring the electrophilic character of the warhead to target specific cysteines, therefore we were inspired to perform a systematic study on a wide set of warheads representing different chemistries. Starting from the available organic chemistry toolbox, we compiled a covalent fragment library that was characterized by non-enzymatic reactivity and selectivity models, and enzyme assays. Our results revealed that similar to Michael acceptors, warheads of other nucleophilic additions, nucleophilic substitutions and oxidations cover the same range of reactivity. This approach allowed us to discover novel reactive MurA inhibitor chemotypes having similar potency as the clinically approved fosfomycin. Investigating a range of warhead chemistries, we found that they show different profiles of

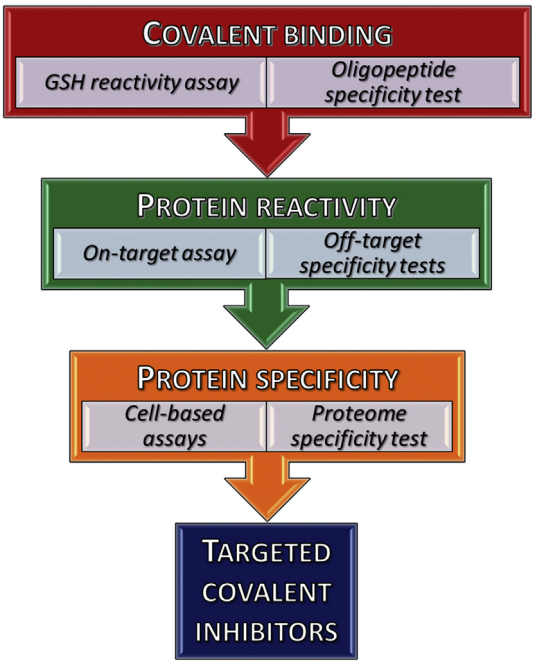


**Fig. 10.** Proposed road map for the selection and prioritization of warheads for TCIs.

functional, enzyme family, species and protein specificities. These findings have been confirmed by characterizing $S_N$ and $Ad_{NM}$ types of fragments and comparing their profiles to proteome-wide affinity data. Analysis of data for a wide range of biological targets suggests that the covalent binding of TCIs is also influenced by the reactivity of the target cysteine, and therefore, no chemistry or warhead could be considered a universal solution for designing covalent inhibitors. Based on these results, we propose a road map for the rational selection and prioritization of warheads for TCIs (Fig. 10).

At the initial phase, the reactivity of potential warheads is first evaluated in the GSH assay selecting those of suitable reactivity. Candidates are then evaluated in the new oligopeptide-based cysteine-selectivity assay prioritizing cysteine selective warheads. Fragments with reactive and selective warheads are next tested against the actual protein target and corresponding off-targets. Finally, active and specific fragment inhibitors should be investigated in cell-based and proteome specificity tests to ensure their specific target engagement. Based on the experience accumulated in our and others labs in academia and industry we believe that the road map suggested here could facilitate the discovery of new covalent inhibitors with improved activity and selectivity.

## 4. Experimental section

### 4.1. Instruments

$^1$H NMR spectra were recorded in DMSO-$d_6$ or $CDCl_3$ solution at room temperature, on a Varian Unity Inova 500 spectrometer (500 MHz for $^1$H NMR spectra), with the deuterium signal of the solvent as the lock and TMS as the internal standard. Chemical shifts ($\delta$) and coupling constants ($J$) are given in ppm and Hz, respectively.

HPLC-MS measurements were performed using a Shimadzu LCMS-2020 device equipped with a Reprospher 100C18 (5 μm; 100 × 3mm) column and positive-negative double ion source (DUIS±) with a quadrupole MS analysator in a range of 50–1000 $m/z$. Sample was eluted with gradient elution using eluent A (10 mM ammonium formate in water:acetonitrile 19:1) and eluent B (10 mM ammonium formate in water:acetonitrile 1:4). Flow rate was set to 1 ml/min. The initial condition was 0% B eluent, followed by a linear gradient to 100% B eluent by 1 min, from 1 to 3.5 min 100% B eluent was retained; and from 3.5 to 4.5 min back to initial condition with 5% B eluent and retained to 5 min. The column temperature was kept at room temperature and the injection volume was 10 μl. Purity of compounds was assessed by HPLC with UV detection at 215 nm; all tested compounds were >95% pure.

A Sciex 6500 QTRAP triple quadrupole – linear ion trap mass spectrometer, equipped with a Turbo V Source in electrospray mode (Sciex, CA, USA) and a Perkin Elmer Series 200 micro LC system (Massachusetts, USA) consisting of binary pump and an autosampler was used for LC–MS/MS analysis. Data acquisition and processing were performed using Analyst software version 1.6.2 (AB Sciex Instruments, CA, USA). Chromatographic separation was achieved by Purospher STAR RP-18 endcapped (50 mm × 2,1 mm, 3 μm) LiChocart® 55-2 HPLC Cartridge. Sample was eluted with gradient elution using solvent A (0.1% formic acid in water) and solvent B (0.1% formic acid in acetonitrile). Flow rate was set to 0.5 ml/min. The initial condition was 5% B for 2 min, followed by a linear gradient to 95% B by 6 min, from 6 to 8 min 95% B was retained; and from 8 to 8.5 min back to initial condition with 5% eluent B and retained to 14.5 min. The column temperature was kept at room temperature and the injection volume was 10 μl. Nitrogen was used as the nebulizer gas (GS1), heater gas (GS2), and curtain gas with the optimum values set at 35, 45 and 45 (arbitrary units), respectively. The source temperature was 450 °C and the ion spray voltage set at 5000 V. Declustering potential value was set to 150 V.

### 4.2. GSH assay

For glutathione assay 500 μM solution of the fragment (PBS buffer pH 7.4, 10% acetonitrile, 250 μL) with 200 μM solution of indoprofen as internal standard was added to 10 mM glutathione solution (dissolved in PBS buffer, 250 μL) in 1:1 ratio. The final concentration was 250 μM fragment, 100 μM indoprofen, 5 mM glutathione and 5% acetonitrile (500 μL). The final mixture was analysed by HPLC-MS after 0, 1, 2, 4, 8, 12, 24, 48, 72 h time intervals. In the case of fragments that were not detectable in a concentration of 250 μM, the final concentrations were reversed, as 5 mM for the fragment and 250 μM for GSH. Degradation kinetic was also investigated respectively using the previously described method, applying pure PBS buffer instead of the glutathione solution. In this experiment the final concentration of the mixture was 250 μM fragment, 100 μM indoprofen and 5% acetonitrile. The AUC (area under the curve) values were determined via integration of HPLC spectra then corrected with internal standard. The fragments AUC values were applied for ordinary least squares (OLS) linear regression and for computing the important parameters (kinetic rate constant, half-life time) a programmed excel (Visual Basic for Applications) was utilized. The data are expressed as means of duplicate determinations, and the standard deviations were within 10% of the given values.

The calculation of the kinetic rate constant for the degradation and corrected GSH-reactivity is the following. Reaction half-life for pseudo-first order reactions is $t_{1/2} = \ln 2/k$, where k is the reaction rate. In the case of competing reactions (reaction with GSH and degradation), the effective rate for the consumption of the starting compound is $k_{eff} = k_{deg} + k_{GSH}$. When measuring half-lives experimentally, the $t_{1/2(eff)} = \ln 2/(k_{eff}) = \ln 2/(k_{deg} + k_{GSH})$. In our case, the corrected $k_{deg}$ and $k_{eff}$ (regarding to blank and GSH containing samples, respectively) can be calculated by linear regression of the

datapoints of the kinetic measurements. The corrected $k_{GSH}$ is calculated by $k_{eff}$-$k_{deg}$, and finally half-life time is determined using the equation $t_{1/2} = \ln 2/k$.

### 4.3. Oligopeptide assay

For nonapeptide assay 2 mM solution of the fragment (PBS buffer pH 7.4 with 20% acetonitrile) was added to 200 μM nonapeptide solution (PBS buffer pH 7.4) in 1:1 ratio. The final assay mixture contained 1 mM fragment, 100 μM peptide and 10% acetonitrile. The samples were incubated at room temperature overnight. Based on the GSH reactivity the applied incubation time was 16 h or 24 h (fragments with less than 12 h half-life time against GSH were incubated for 16 h, the others for 24 h). Information Dependent Acquisition (IDA) LC-MS/MS experiment was used to identify if the fragment binding was specific to thiol residues or not. Enhanced MS scan was applied as survey scan and enhanced product ion (EPI) was the dependent scan. The collision energy in EPI experiments was set to 30eV with collision energy spread (CES) of 10 V. The identification of the binding position of the fragments to the nonapeptide was performed by GPMAW 4.2. software. Relative quantitation of the nonapeptide − fragment covalent conjugates was calculated from the total ion chromatograms (based on peak area of the selected ion chromatograms).

### 4.4. MurA assay

$MurA_{EC}$ and $MurA_{SA}$ proteins were recombinant, expressed in *E. coli.* [53] The inhibition of MurA was monitored with the colorimetric malachite green method in which orthophosphate generated during reaction is measured. MurA enzyme (*E. coli* or *S. aureus*) was pre-incubated with the substrate UNAG and compound for 30 min at 37 °C. The reaction was started by the addition of the second substrate PEP, resulting in a mixture with final volume of 50 μl. The mixtures contained: 50 mM Hepes, pH 7.8, 0.005% Triton X-114, 200 μM UNAG, 100 μM PEP, purified MurA (diluted in 50 mM Hepes, pH 7.8, with 1 mM DTT or without DTT or with 5 mM cysteine) and 100 μM of each tested compound dissolved in DMSO. All compounds were soluble in the assay mixtures containing 5% DMSO (v/v). After incubation for 15 min at 37 °C, the enzyme reaction was terminated by adding Biomol® reagent (100 μL) and the absorbance was measured at 650 nm after 5 min. All of the experiments were run in duplicate. Residual activities (RAs) were calculated with respect to similar assays without the tested compounds and with 5% DMSO. The $IC_{50}$ values, the concentration of the compound at which the residual activity was 50%, were determined by measuring the residual activities at seven different compound concentrations. The data are expressed as means of duplicate determinations, and the standard deviations were within 10% of the given values. Time dependent inhibition assay was also performed. The applied time intervals of preincubation were 0, 10, 20, 30, 40, 50, 60 min. Concentration of each compounds was around determined $IC_{50}$ values (at 30 min of preincubation). For dilution assay the practical concentration of the fragments was the $IC_{50}$ value (determined at 30 min of preincubation) tenfold, in the case where concentration of inhibitor was lower than concentration of enzyme, the equimolar concentrations of enzyme and inhibitor was used (25 μM). The applied concentration of enzyme was the usual concentration in the reactivity assays hundredfold (25 μM). After 30 min of preincubation the mixture was diluted hundredfold, then the previously described reactivity assay was stared with PEP.

### 4.5. Cathepsin B assay

The protein was recombinant, expressed in *E. coli.* [54] For endopeptidase reactivity assay 215 μL of cathepsin B (5 nM) was preincubated with 11.94 μL of compound (105 μM final concentration) for 30 min at 37 °C with gentle shaking. 95 μL of the mixture (100 μM final compound concentration) was added to a black 96-well plate with 5 μL of the Z-RR-AMC (Bachem) substrate (5 μM final concentration). Final concentration of DMSO in assay mixture was 5%. As control 5% DMSO in assay buffer was used. The reaction was continuously monitored at 460 nm ± 10 nm with excitation at 380 nm ± 20 nm and 37 °C. The practical assay buffer was 100 mM phosphate buffer, pH 6.0 with 0.01% Triton X-100, 5 mM cysteine, 1.5 mM EDTA and 0.1% PEG 8000. For exopeptidase reactivity assay 215 μL of cathepsin B (0.5 nM) was preincubated with 11.94 μL of compound (105 μM final concentration) for 30 min at 37 °C with gentle shaking. 95 μL of the mixture (100 μM final compound concentration) was added to a black 96-well plate with 5 μL of the Abz-GIVRAK(Dnp)-OH (Bachem) substrate (1 μM final concentration). Final concentration of DMSO in assay mixture was 5%. As control 5% DMSO in assay buffer was used. The reaction was continuously monitored at 420 nm ± 10 nm with excitation at 320 nm ± 20 nm and 37 °C. The practical assay buffer was 60 mM acetate buffer, pH 5.0 with 0.01% Triton X-100, 5 mM cysteine, 1.5 mM EDTA and 0.1% PEG 8000.

### 4.6. Cathepsin X assay

Cathepsin X protein was recombinant, expressed in *Pichia pastoris* [55]. For the assay 215 μL of cathepsin X (20 nM) was preincubated with 11.94 μL of compound (105 μM final concentration) for 30 min at 37 °C with gentle shaking. 95 μL of the mixture (100 μM final compound concentration) was added to a black 96-well plate with 5 μL of the Abz-FEK(Dnp)-OH [56] substrate (3.25 μM final concentration). Final concentration of DMSO in assay mixture was 5%. As control 5% DMSO in assay buffer was used. The reaction was continuously monitored at 420 nm ± 10 nm with excitation at 320 nm ± 20 nm and 37 °C. The practical assay buffer was 100 mM Na acetate buffer, pH 5.5 with 0.01% Triton X-100, 5 mM cysteine, 1.5 mM EDTA and 0.1% PEG 8000.

### 4.7. Thrombin assay

Spectrophotometric enzyme tests was performed in transparent microtiter plates in a final volume of 200 μL. The reaction rates in the absence and in the presence of the inhibitor was measured. 50 μL HEPES buffer (10 mM Hepes buffer (HEPES, Sigma); 150 mM NaCl, adjusted with 0,1 M NaOH to pH 7.5), 50 μL solution (2% DMSO in water) of different inhibitors at 400 μM (in case of measurement without inhibitor water) and 50 μL of thrombin solution (human thrombin, Sigma-Aldrich, 2 NIH E/mL) was pipetted into the microtiter plate. The plate was incubated for 30 min at 25 °C and subsequently 50 μL chromogenic substrate (S-2238 (H-D-Phe-Pip-Arg-pNA•2HCl, Chromogenix),160 μM) was added. Final concentration of the inhibitors was 100 μM, DMSO 0,5%, thrombin 0,5 NIH E/mL and substrate 40 μM. The microtiter plate was put into the spectrophotometer (Biotek H4) and the increase of absorbance at 405 nm at 25 °C was measured every 10 s. Change of absorbance form the initial, linear part of the curve was used to determine residual activity; measurements were carried out in triplicate in two independent experiments. For the comparison assay, cysteine was added to the buffer (15 mM), resulting in incubation mixture containing 5 mM cysteine.

### 4.8. MurA proteomics MS/MS

For the MurA labelling experiment the 42 μM stock solution of

$MurA_{EC}$ in 20 mM Hepes at pH 7.2–7.4 with 1 mM DTT was filtered through a G25 column and the medium was changed to 50 mM Tris with 0.005% Triton X-100 at pH 8.0. For the activation of the enzyme 1 mg UDPNAG was added as a solid to reach 40 mM concentration and the mixture was incubated at 37 °C for 30 min. Fragments were added from a 250 mM DMSO stock diluted in the labelling solution to 5 mM. The incubation was continued at 37 °C for additional 30 min. After the labelling, the mixture was purified on a G25 column. Briefly 40–50 μL of the sample and 10 μL 0.2% (w/v) RapiGest SF (Waters, Milford, USA) solution buffered with 50 mM ammonium bicarbonate were mixed (pH = 7.8) and 3,3 μL of 45 mM DTT in 100 mM $NH_4HCO_3$ were added and kept at 37.5 °C for 30 min. After cooling the sample to room temperature, 4.16 μL of 100 mM iodoacetamide in 100 mM $NH_4HCO_3$ were added and placed in the dark in room temperature for 30 min. The reduced and alkylated protein was then digested by 10 μL (1 mg $mL^{-1}$) trypsin (the enzyme-to-protein ratio was 1: 10) (Sigma, St Louis, MO, USA). The sample was incubated at 37 °C for overnight. To degrade the surfactant, 7 μL of formic acid (500 mM) solution was added to the digested MurA sample to obtain the final 40 mM concentration (pH ≈ 2) and was incubated at 37 °C for 45 min. For LC-MS analysis, the acid treated sample was centrifuged for 5 min at 13 000 rpm. QTRAP 6500 triple quadruple – linear ion trap mass spectrometer, equipped with a Turbo V source in electrospray mode (AB Sciex, CA, USA) and a Perkin Elmer Series 200 micro LC system (Massachusetts, USA) was used for LC-MS/MS analysis. Data acquisition and processing were performed using Analyst software version 1.6.2 (AB Sciex Instruments, CA, USA). Chromatographic separation was achieved by using the Vydac 218 TP52 Protein & Peptide C18 column (250 mm × 2.1 mm, 5 μm). The sample was eluted with a gradient of solvent A (0.1% formic acid in water) and solvent B (0.1% formic acid in ACN). The flow rate was set to 0.2 mL min−1. The initial conditions for separation were 5% B for 7 min, followed by a linear gradient to 90% B by 53 min, from 60 to 63 min 90% B is retained; from 64 to 65 min back to the initial conditions with 5% eluent B retained to 70 min. The injection volume was 10 μL (300 pmol on the column). Information Dependent Acquisiton (IDA) LC-MS/MS experiment was used to identify the modified tryptic MurA peptide fragments. Enhanced MS scan (EMS) was applied as survey scan and enhanced product ion (EPI) was the dependent scan. The collision energy in EPI experiments was set to rolling collision energy mode, where the actual value was set on the basis of the mass and charge state of the selected ion. Further IDA criteria: ions greater than: 400.000 *m*/*z*, which exceeds106 counts, exclude former target ions for 30 s after 2 occurrence(s). In EMS and in EPI mode the scan rate was 1000 Da/s as well. Nitrogen was used as the nebulizer gas (GS1), heater gas (GS2), and curtain gas with the optimum values set at 50, 40 and 40 (arbitrary units). The source temperature was 350 °C and the ion spray voltage set at 5000 V. Declustering potential value was set to 150 V. GPMAW 4.2. software and ProteinProspector (http://prospector.ucsf.edu/prospector/mshome.htm) was used to analyse the large number of MS/MS spectra and identify the modified tryptic MurA peptides.

## Funding sources

This study was primarily supported by the National Brain Research Program grants (projects KTIA NAP_13 and project 2017-1.2.1-NKP-2017-00002) and MSCA ETN FRAGNET (project 675899) grant to G. M. Keserű. The project was also funded by the Hungarian Science Foundation OTKA (project K116904) and Hungarian Academy of Sciences postdoctoral fellowship to P. Ábrányi-Balogh and Bolyai fellowship to K. Horváti. Additional support was provided by the Slovenian Research Agency (projects P4-0127, P1-0208 and L1-6745).

## Acknowledgement

We thank I. Pápai (RCNS, Hungary), D. Menyhárd (ELTE, Hungary), G. Makara (ChemPass, Hungary), M. M. Hann (GlaxoSmithKline, UK), X. Barril (University of Barcelona, Spain) and R. Hubbard (University of York, UK) for their comments on the manuscript.

## Appendix A. Supplementary data

Supplementary data to this article can be found online at https://doi.org/10.1016/j.ejmech.2018.10.010.

## References

[1] T.A. Baillie, Targeted covalent inhibitors for drug design, Angew. Chem. Int. Ed. Engl. Transl 55 (2016) 13408–13421.
[2] D.A. Shannon, E. Weerapana, Covalent protein modification: the current landscape of residue-specific electrophiles, Curr. Opin. Chem. Biol. 24 (2015) 18–26.
[3] a) A. Miseta, P. Csutora, Relationship Between the Occurrence of Cysteine in Proteins and the Complexity of Organisms, Mol. Biol. Evol. 17 (2000) 1232–1239;
b) K.K. Hallenbeck, D.M. Turner, A.R. Renslo, M.R. Arkin, Targeting non-catalytic cysteine residues through structure-guided drug discovery, Curr. Top. Med. Chem. 17 (2017) 4–15.
[4] Z. Zhao, P.E. Bourne, Progress with covalent small-molecule kinase inhibitors, Drug Discov. Today 23 (2018) 727–735.
[5] R. Lagoutte, R. Patouret, N. Winssinger, Covalent inhibitors: an opportunity for rational target selectivity, Curr. Op. Chem. Biol. 39 (2017) 54–63.
[6] N.J. Pace, E. Weerapana, Diverse functional roles of reactive cysteines, ACS Chem. Biol. 8 (2013) 283–296.
[7] E. Weerapana, C. Wang, G.M. Simon, F. Richter, S. Khare, M.B. Dillon, D.A. Bachovchin, K. Mowen, D. Baker, B.F. Cravatt, Quantitative reactivity profiling predicts functional cysteines in proteomes, Nature 468 (2010) 790–795.
[8] C. Hu, X. Dong, C. Hu, X. Dong, Cysteine-targeted irreversible inhibitors of tyrosine kinases and key interactions, Curr. Med. Chem. (2018), https://doi.org/10.2174/0929867325666180713124223.
[9] A. Chaikuad, P. Koch, S.A. Laufer, S. Knapp, The cysteinome of protein kinases as a target in drug development, Angew. Chem., Int. Ed. Engl. 57 (2018) 4372–4385.
[10] J. Singh, R.C. Petter, T.A. Baillie, A. Whitty, The resurgence of covalent drugs, Nat. Rev. Drug Discov. 10 (2011) 307–317.
[11] R.A. Bauer, Covalent inhibitors in drug discovery: from accidental discoveries to avoided liabilities and designed therapies, Drug Discov. Today 20 (2015) 1061–1073.
[12] J.M. Bradshaw, J.M. McFarland, V.O. Paavilainen, A. Bisconte, D. Tam, V.T. Phan, S. Romanov, D. Finkle, J. Shu, V. Patel, T. Ton, X. Li, D.G. Loughhead, P.A. Nunn, De E. Karr, M.E. Gerritsen, J.O. Funk, T.D. Owens, E. Verner, K.A. Brameld, R.J. Hill, D.M. Goldstein, J. Taunton, Prolonged and tunable residence time using reversible covalent kinase inhibitors, Nat. Chem. Biol. 11 (2015) 525–531.
[13] J. Engel, A. Richters, M. Getlik, S. Tomassi, M. Keul, M. Termathe, J. Lategahn, C. Becker, S. Mayer-Wrangowski, C. Grütter, N. Uhlenbrock, J. Krüll, N. Schaumann, S. Eppmann, P. Kibies, F. Hoffgaard, J. Heil, S. Menninger, S. Ortiz-Cuaran, J.M. Heuckmann, V. Tinnefeld, R.P. Zahedi, M.L. Sos, C. Shultz-Fademrecht, R.K. Thomas, S.M. Kast, D. Rauh, Targeting drug resistance in EGFR with covalent inhibitors: a structure-based design approach, J. Med. Chem. 58 (2015) 6844–6863.
[14] D.S. Johnson, E. Weerapana, B.F. Cravatt, Strategies for discovering and derisking covalent, irreversible enzyme inhibitors, Future Med. Chem. 2 (2010) 949–964.
[15] R.A. Thompson, E.M. Isin, M.O. Ogese, J.T. Mettetal, D.P. Williams, Reactive metabolites: current and emerging risk and hazard assessments, Chem. Res. Toxicol. 29 (2016) 505–533.
[16] I.M. Serafimova, M.A. Pufall, S. Krishnan, K. Duda, M.S. Cohen, R.L. Maglathlin, J.M. McFarland, R.M. Miller, M. Frödin, J. Taunton, Reversible targeting of noncatalytic cysteines with chemically tuned electrophiles, Nat. Chem. Biol. 8 (2012) 471–476.
[17] J. Du, X. Yan, Z. Liu, L. Cui, P. Ding, X. Tan, X. Li, H. Zhou, Q. Gu, J. Xu, cBinderDB: a covalent binding agent database, Bioinformatics 33 (2017) 1258–1260.
[18] S.G. Kathman, A.V. Statsyuk, Covalent tethering of fragments for covalent probe discovery, Med. Chem. Commun. 7 (2016) 576–585.
[19] M. Gersch, J. Kreuzer, S.A. Sieber, Electrophilic natural products and their biological targets, Nat. Prod. Rep. 29 (2012) 659–682.
[20] M.E. Flanagan, J.A. Abramite, D.P. Anderson, A. Aulabaugh, U.P. Dahal, A.M. Gilbert, C. Li, J. Montgomery, S.R. Oppenheimer, T. Ryder, B.P. Schuff, D.P. Uccello, G.S. Walker, Y. Wu, M.F. Brown, J.M. Chen, M.M. Hayward, M.C. Noe, R.S. Obach, L. Philippe, V. Shanmugashundaram, M.J. Shapiro,

J. Starr, J. Stroh, Y. Che, Chemical and computational methods for the characterization of covalent reactive groups for the prospective design of irreversible inhibitors, J. Med. Chem. 57 (2014) 10072–10079.
[21] S.G. Kathman, Z. Xu, A.V. Statsyuk, A fragment–based method to discover irreversible covalent inhibitors of cysteine proteases, J. Med. Chem. 57 (2014) 4969–4974.
[22] R.M. Miller, V.O. Paavilainen, S. Krishnan, I.M. Serafimova, J. Taunton, Electrophilic fragment–based design of reversible covalent kinase inhibitors, J. Am. Chem. Soc. 135 (2013) 5298–5301.
[23] G.G. Ferenczy, G.M. Keserű, Thermodynamics of fragment binding, J. Chem. Inf. Model. 52 (2012) 1039–1045.
[24] D.A. Erlanson, S.W. Fesik, R.E. Hubbard, W. Jahnke, H. Jhoti, Twenty years on: the impact of fragments on drug discovery, Nat. Rev. Drug Discov. 15 (2016) 605–619.
[25] R. Lonsdale, J. Burgess, N. Colclough, N.L. Davies, E.M. Lenz, A.L. Orton, R.A. Ward, Relationship Between the Occurrence of Cysteine in Proteins and the Complexity of Organisms, J. Chem. Inf. Model. 57 (2017) 3124–3137.
[26] N. Fuller, L. Spadola, L.,S. Cowen, J. Patel, H. Schönherr, Q. Cao, A. McKenzie, F. Edfeldt, A. Rabow, R. Goodnow, An improved model for fragment-based lead generation at AstraZeneca, Drug Discov. Today 21 (2016) 1272–1283.
[27] G.M. Keserű, D.A. Erlanson, G.G. Ferenczy, M.M. Hann, C.W. Murray, S.D. Pickett, Design principles for fragment libraries: maximizing the value of learnings from pharma fragment-based drug discovery (FBDD) programs for use in academia, J. Med. Chem. 59 (2016) 8189–8206.
[28] Z. Miller, L. Ao, K.B. Kim, W. Lee, Inhibitors of the immunoproteasome: current status and future directions, Curr. Pharmaceut. Des. 19 (2013) 4140–4151.
[29] L.L. Silver, Does the cell wall of bacteria remain a viable source of targets for novel antibiotics? Biochem. Pharmacol. 71 (2006) 996–1005.
[30] A. El Zoeiby, F. Sanschagrin, R.C. Levesque, Structure and function of the Mur enzymes: development of novel inhibitors, Mol. Microbiol. 47 (2003) 1–12.
[31] M. Hrast, I. Sosič, R. Sink, S. Gobec, Inhibitors of the peptidoglycan biosynthesis enzymes MurA-F, Bioorg. Chem. 55 (2014) 2–15.
[32] C.J. Dunsmore, K. Miller, K.L. Blake, S.G. Patching, P.J. Henderson, J.A. Garnett, W.J. Stubbings, S.E. Phillips, D.J. Palestrant, J. De Los Angeles, J.A. Leeds, I. Chopra, C.W. Fishwick, 2-Aminotetralones: novel inhibitors of MurA and MurZ, Bioorg. Med. Chem. Lett 18 (2008) 1730–1734.
[33] Y. Zhong, Y. Xu, E.V. Anslyn, Studies of reversible conjugate additions, Eur. J. Org Chem. (2013) 5017–5021.
[34] Y. Zhou, L. Li, H. Ye, L. Zhang, L. You, Quantitative reactivity scales for dynamic covalent and systems chemistry, J. Am. Chem. Soc. 138 (2016) 381–389.
[35] K. Doyle, H. Lönn, H. Käck, A. van de Poel, S. Swallow, P. Gardiner, S. Connoly, J. Root, C. Wikell, G. Dahl, K. Stenvall, P. Johanesson, Discovery of second generation reversible covalent DPP1 inhibitors leading to an oxazepane amidoacetonitrile based clinical candidate (AZD7986), J. Med. Chem. 59 (2016) 9457–9472.
[36] B. Bian, S. Mongrain, S. Cagnol, M.J. Langlois, J. Boulanger, G. Bernatchez, J.C. Carrier, F. Boudreau, N. Rivard, Cathepsin B promotes colorectal tumorigenesis, cell invasion, and metastasis, Mol. Carcinog. 55 (2016) 671–687.
[37] J. Kos, A. Mitrović, B. Mirković, The current stage of cathepsin B inhibitors as potential anticancer agents, Future Med. Chem. 6 (2014) 1355–1371.
[38] O.C. Olson, J.A. Joyce, Cysteine cathepsin proteases: regulators of cancer progression and therapeutic response, Nat. Rev. Canc. 15 (2015) 712–729.
[39] P. Schenker, P. Alfarano, P. Kolb, A. Caflisch, A. Baici, A double-headed cathepsin B inhibitor devoid of warhead, Proteome Sci. 17 (2008) 2145–2155.
[40] M. Siklos, M. BenAissa, G.R.J. Thatcher, Cysteine proteases as therapeutic targets: does selectivity matter? A systematic review of calpain and cathepsin inhibitors, Acta Pharm. Sin. B 5 (2015) 506–519.
[41] A. Pišlar, B. Božić, N. Zidar, J. Kos, Inhibition of cathepsin X reduces the strength of microglial-mediated neuroinflammation, Neuropharmacology 114 (2017) 88–100.
[42] D.K. Nägler, S. Krüger, A. Kellner, E. Ziomek, R. Menard, P. Buhtz, M. Krams, A. Roessner, U. Kellner, Up-regulation of cathepsin X in prostate cancer and prostatic intraepithelial neoplasia, Prostate 60 (2014) 109–119.
[43] C. Therrien, P. Lachance, T. Sulea, E.Q. Purisima, H. Qi, E. Ziomek, A. Alvarez-Hernandez, W.R. Roush, R. Ménard, Cathepsins X and B can be differentiated through their respective mono- and dipeptidyl carboxypeptidase activities, Biochemist 40 (2001) 2702–2711.
[44] K.L. Blake, A.J. O'Neill, D. Mengin-Lecreulx, P.J. Henderson, J.M. Bostock, C.J. Dunsmore, K.J. Simmons, C.W. Fishwick, J.A. Leeds, I. Chopra, The nature of Staphylococcus aureus MurA and MurZ and approaches for detection of peptidoglycan biosynthesis inhibitors, Mol. Microbiol. 72 (2009) 335–343.
[45] D. Musil, D. Zucic, D. Turk, R.A. Engh, I. Mayr, R. Huber, T. Popovic, V. Turk, T. Towatari, N. Katunuma, A X-ray crystal structure of human liver cathepsin B: the structural basis for its specificity, EMBO J. 10 (1991) 2321–2330.
[46] F. Krekel, A.K. Samland, P. Macheroux, N. Amrhein, J.N.S. Evans, Determination of the pKa value of C115 in MurA (UDP-N-acetylglucosamine enolpyruvyl-transferase) from Enterobacter cloacae, Biochemist 39 (2000) 12671–12677.
[47] M. Sivaraja, N. Pozzi, M. Rienzo, K. Lin, T.P. Shiau, D.M. Clemens, L. Igoudin, P. Zalicki, S.S. Chang, M. Angels Estiarte, K.M. Short, D.C. Williams, A. Datta, E. Di Cera, D.B. Kita, Reversible covalent direct thrombin inhibitors, PloS One 13 (8) (2018), e0201377, https://doi.org/10.1371/journal.pone.0201377.
[48] K.M. Backus, B.E. Correia, K.M. Lum, S. Forli, B.D. Horning, G.E. González-Páez, S. Chatterjee, B.R. Lanning, J.R. Teijaro, A.J. Olson, D.W. Wolan, B.F. Cravatt, Proteome-wide covalent ligand discovery in native biological systems, Nature 534 (2016) 570–574.
[49] R.D. Little, M.R. Masjedizadeh, O. Wallquist, J.I. McLoughlin, The intramolecular Michael reaction, Org. React. 47 (1995) 315–552.
[50] S.R. Hartshorn, Aliphatic Nucleophilic Substitution, Cambridge University Press, London, 1973.
[51] D.P. Nair, M. Podgórski, S. Chatani, T. Gong, W. Xi, C.R. Fenoli, C.N. Bowman, The thiol–michael addition click reaction: a powerful and widely used tool in materials chemistry, Chem. Mater. 26 (2014) 724–744.
[52] C.G. Parker, A. Galmozzi, Y. Wang, B.E. Correira, K. Sasaki, C.M. Joslyn, A.S. Kim, C.L. Cavallaro, R.M. Lawrence, S.R. Johnson, I. Narvaiza, E. Saez, B.F. Cravatt, Ligand and target discovery by fragment-based screening in human cells, Cell 168 (2017) 527–541.
[53] K. Rožman, S. Lešnik, B. Brus, M. Hrast, M. Sova, D. Patin, H. Barreteau, J. Konc, D. Janežič, S. Gobec, Discovery of new MurA inhibitors using induced-fit simulation and docking, Bioorg. Med. Chem. Lett 27 (2017) 944–949.
[54] R. Kuhelj, M. Dolinar, J. Pungercar, V. Turk, The preparation of catalytically active human cathepsin B from its precursor expressed in Escherichia coli in the form of inclusion bodies, Eur. J. Biochem. 229 (1995) 533–539.
[55] U. Pečar Fonović, J. Kos, Efficient removal of cathepsin L from active cathepsin X using immunoprecipitation technique, Acta Chim. Slov. 56 (2009) 985–988.
[56] L. Puzer, S.S. Cotrin, M.H. Cezari, I.Y. Hirata, M.A. Juliano, I. Stefe, D. Turk, B. Turk, L. Juliano, A.K. Carmona, Recombinant human cathepsin X is a carboxymonopeptidase only: a comparison with cathepsins B and L, Biol. Chem. 386 (2005) 1191–1195.